# Imaging Glioma Extent with $^{131}$I-TM-601

David C. Hockaday, BS[1]; Sui Shen, PhD[2]; John Fiveash, MD[2]; Andrew Raubitschek, MD[3]; David Colcher, PhD[3]; An Liu, PhD[3]; Vern Alvarez, PhD[4]; and Adam N. Mamelak, MD[1]

*[1]Neurosurgery Section, Department of General and Oncological Surgery, City of Hope Cancer Center, Duarte, California; [2]Department of Radiation Oncology, University of Alabama at Birmingham, Birmingham, Alabama; [3]Department of Radio-Immunotherapy, Beckman Research Institute, City of Hope Cancer Center, Duarte, California; and [4]Transmolecular, Inc., Birmingham, Alabama*

TM-601, a 36-amino-acid peptide, selectively binds to glioma cells but not normal brain parenchyma. A phase I/II clinical trial of intracavitary $^{131}$I-TM-601 in adult patients with recurrent high-grade glioma was performed to determine the biodistribution and toxicity of this potential therapy. We evaluated imaging and biodistribution data from this trial to assess whether $^{131}$I-TM-601 might be useful in determining tumor extent. **Methods:** Adult patients with recurrent high-grade gliomas underwent tumor resection, implantation of an intracavitary reservoir, and a single-dose injection of 370 MBq (10 mCi) $^{131}$I-TM-601 (0.25–1.0 mg of $^{131}$I-TM-601) 2–4 wks after surgery. Total-body planar scans and whole-brain SPECT scans were obtained on days 0, 1, 2, 3, and 6–8 after injection. Postresection MR images were coregistered to the SPECT scans using image analysis software. Analysis of the rate of radioactive decay and biologic elimination from the body and at the cavity site was performed. T1-weighted with gadolinium contrast (T1-Wc), T2-weighted (T2), and SPECT volumes were estimated by stereological Cavalieri sections and compared for overlap. **Results:** Nonbound $^{131}$I-TM-601 was eliminated by 48 h after injection with the remaining radiolabeled peptide bound to tumor for at least 6–8 d. Biologic decay rates from 24 to 168 h after injection were only slightly shorter than the physical decay of $^{131}$I (6.3 vs. 8.0 d). A comparison of tumor volume estimates using all 3 imaging parameters indicated that $^{131}$I-TM-601–determined tumor volumes more closely paralleled T2 volumes than T1-Wc volumes. Overlap between coregistered MRI and SPECT scans corroborated the presence of radiolabeled peptide in the vicinity of infiltrating tumor up to 168 h after injection. **Conclusion:** $^{131}$I-TM-601 provides a reliable estimate for primary tumor extent. Further modification of this radiopeptide with other better imaging isotopes may provide an important tool for determining tumor extent and differentiating regions of viable tumor from necrosis.

**Key Words:** glioma; imaging; chlorotoxin; TM-601; SPECT

**J Nucl Med 2005; 46:580–586**

Gliomas are the most common primary brain tumors diagnosed annually, comprising nearly 16,500 cases and accounting for nearly 13,000 deaths (*1,2*). The most lethal gliomas are the high-grade gliomas (HGGs): grade III anaplastic astrocytoma, anaplastic oligoendroglioma, and grade IV gliomablastoma multiforme (GBM). Around 80% of all HGGs are GBMs, which frequently display a rim of vascular and cellular proliferation and edema around a dark necrotic core. With a 2-y survival rate of <9% and a 5-y survival rate of <4%, the prognosis for GBM has not substantially improved over the past 2 decades (*1,2*)

The ability to adequately image the tumor volume and the extent of infiltration into normal brain parenchyma is critical for treatment since upwards of 85% of HGG patients have recurrences near the original tumor site and the extent of tumor resection is one of the most important predictors of long-term survival (*3–5*). Accurate determination of tumor extent is important in maximizing surgical resection and radiotherapy treatment fields and is becoming increasingly important for convection-enhanced local delivery of therapies via intraparenchymal catheters. Traditional imaging methods such as MRI, magnetic resonance spectroscopy (MRS), and $^{18}$F-FDG PET do not adequately define the extent of glioma invasion or the tumor response to therapy. $^{18}$F-FDG is a nonspecific measure of glucose utilization. Because the brain relies on glucose as its sole source of energy, normal brain parenchyma is not well differentiated from invading tumor and, in some cases, takes up more radioactivity than the tumor. PET has a relatively low spatial resolution and, as such, poorly identifies regions of tumor <1.5 cm in size. Several reports indicate that though PET is reasonably sensitive (81%–86%) in detecting recurrent tumor after irradiation, it is not very specific (22%–40%) (*6,7*). $^{1}$H-MRS can differentiate tumor from nonneoplastic processes with greater accuracy than PET, with sensitivities in the range of 79%–100% and specificities in the range of 74%–100% (*8–10*). Nonetheless, $^{1}$H-MRS lacks spatial resolution, and many sections of the brain are difficult to image due to bony artifacts, fluid and fat interfaces, or magnetic field inhomogeneities of degraded spectral quality. These properties make it unrealistic for accurate assessment of tumor extent. MRI remains the principal modality for imaging of gliomas with superb spatial resolution. However, conventional MRI is unable to distinguish viable tumor from radionecrosis and infiltrating tumor from cerebral edema.

Received Jun. 25, 2004; revision accepted Nov. 2, 2004.

For correspondence or reprints contact: Adam N. Mamelak, MD, Neurosurgery Section, Medical Office Building L002, City of Hope Cancer Center, 1500 E. Duarte Rd. Duarte, CA 91010.

E-mail: amamelak@coh.org

Studies have shown that the combined use of these modalities better predicts sites of recurrence than T1- or T2-weighted MRI alone (*11–13*). Distinguishing viable tumor from vasogenic edema or necrosis, however, remains difficult—even with metabolic imaging agents—due to the significant amount of angiogenesis present in high-grade gliomas and breaches of the blood–brain barrier (BBB) at the edema site.

Tumor-specific and rapidly diffusible radiolabeled targeting molecules can address this problem for the imaging of HGG. Most of the currently available radiopharmaceuticals are either too large to negotiate the BBB and the interstices of the extracellular matrix or they are not specific in their binding to glioma. Monoclonal antibodies (mAbs) such as 81C6, for instance, have shown targeting to glioma; however, they are too large to pass the BBB and diffuse from the surgically created resection cavity into the parenchyma, where residual tumor may thrive (*9*). Moreover, most mAbs lack glioma specificity and have a high degree of catabolism of the radiolabel (*14*).

Chlorotoxin (CTX), a scorpion-derived 36-amino-acid peptide, has been shown to specifically bind to the putative MMP2 receptor, which is considered a chloride channel–associated receptor believed to indirectly regulate the chloride channels expressed by gliomas but not normal human cells (*11,15–17*). Currently, it is believed that these chloride channels affect the shape and volume of the cytoskeleton of gliomas and play a key role in tumor infiltration. Several immunohistochemical, in vitro, and in vivo experiments indicate that CTX does not bind to normal brain parenchyma or endothelial cells but specifically binds to tumescent glial cells. TM-601 (Food and Drug Administration [FDA] Investigational New Drug no. 63,030; Transmolecular, Inc.)—a synthetic version of CTX—has been shown to selectively label human gliomas in vivo and in vitro and to demonstrate all of the physical and biologic activities of naturally occurring chlorotoxin. Unlike many other radioligands, TM-601 is relatively small at ~4 kDa: It passes the BBB and diffuses readily through the brain parenchyma and may spread across the entire tumor. Animal experiments indicate that ~15% of an intravenous dose of $^{125}$I-TM-601 crosses the BBB and is taken up by intracranial glioma xenografts in athymic nude mice (Transmolecular, Inc., unpublished data, June 2003).

These properties make TM-601 potentially useful for imaging as well as for targeted local therapy. Several immunohistochemical and radiolabeled cell-binding assays demonstrated a positive correlation between peptide–glioma binding and increasing tumor malignancy (*17*). Biodistribution and dosimetry studies of $^{131}$I-TM-601 in athymic nude mice with intracranially implanted human glioma xenografts suggest no measurable binding of TM-601 in normal tissues (*13*). These findings and supporting in vivo efficacy and toxicology data in animals justified a phase I/II clinical trial of TM-601 conjugated to $^{131}$I and delivered intracranially to patients with recurrent high-grade glioma (City of Hope Institutional Review Board no. 01108). The primary goals of this study were to determine the biodistribution of $^{131}$I-TM-601 and any drug-related toxicity.

The imaging and biodistribution data from a subset of these patients treated at City of Hope Cancer Center were analyzed to determine the potential of radiolabeled TM-601 as a tumor-specific imaging agent for glioma.

## MATERIALS AND METHODS

All patients were treated under an FDA and City of Hope Institutional Review Board–approved protocol (no. 01108), with informed consent. Protocol eligibility criteria and details of the clinical trial are presented in detail elsewhere. Briefly, eligible patients were adults (≥18 y of age), with pathologically verified recurrent high-grade glioma. Patients had unifocal tumors in the cerebral hemispheres and were deemed to be candidates for cytoreductive brain surgery based on tumor size and location and clinical status. Recurrent tumor was pathologically verified during surgery, maximal cytoredcutive surgery was performed, and a catheter and subcutaneous reservoir system (Rickham Reservoir; Codman Shurtleff, Inc.) were implanted. Two to 4 wk after surgery, patients received a single dose injection of 370 ± 37 MBq (10 ± 1 mCi) $^{131}$I-TM-601 (0.25–1.0 mg) through the Rickham reservoir in a volume of 2–5 mL, followed by serial daily total-body planar scans and whole-brain SPECT scans as described.

### Preparation of $^{131}$I-TM-601

Presealed, sterilized vials containing lyophilized TM-601 were radiolabeled with 370 MBq (10 mCi) $^{131}$I via the IODO-GEN bead method (*18*). The extent of labeling was determined via immediate thin-layer chromatography with >92% efficiency required to justify human use.

### Preliminary Scans

Before delivery of $^{131}$I-TM-601 to the patient, a 1-mL volume of 3.7–37 MBq (0.1–1 mCi) $^{111}$In-diethylenetriaminepentaacetic acid ($^{111}$In-DTPA) was injected into the reservoir to ensure catheter patency. At the time of $^{111}$In-DTPA administration, a 256 × 256 matrix image was taken with a γ-camera equipped with a high-energy (247 keV, 15% window) collimator to monitor delivery of the $^{111}$In-DTPA via catheter and observe any leakage. Upon completion, dynamic planar images of the head were continuously acquired for 15 min.

A $^{57}$Co transmission scan was performed with and without the patient on the scanner bench to normalize subsequent imaging data acquired for total-body planar images. Before injection, the $^{57}$Co source was placed ~3 cm below the scanner table with the anterior camera 3 cm above the patient. A high-energy collimator centered at 122 keV with a 20% window was used and images were acquired with a gantry speed of 10 cm/min and 256 × 1,024 matrix size.

### Injection of Radiolabeled Peptide

One to 2 h after labeling, patients received $^{131}$I-TM-601 intracranially via a 25-gauge butterfly needle and a shielded 5-mL syringe in a volume of 2–5 mL inserted into the Rickham reservoir. Initially, 25% of the total radiolabeled peptide dose was given. The patient was observed for 5 min, after which the remaining dose was administered, followed by a 1- to 2-mL saline flush. Blood and urine samples were collected for biodistribution assays. Urine

samples were also collected over the period of days 1–2, 2–3, 3–4, and 4–6 or day 8, whereas blood samples were collected at 1, 2, and 4 h after completion of the infusion and on days 2, 3, and 4 and at the time of imaging on day 6 or day 8.

### Planar Images

After intracranial injection of $^{131}$I-TM-601, anterior and posterior whole-body planar images of matrix size 1,024 × 256 were acquired with a gantry speed of 6 cm/min on a dual-detector γ-camera equipped with a high-energy collimator set at 364 keV (15% window). Image acquisition included a 20-mL, 7.4-MBq (200 μCi) calibrated $^{131}$I source, which had been placed ~10 cm from the feet of the patient. Subsequent images were acquired on days 2, 3, and 4 and either on day 6 or day 8 after injection.

### SPECT

A 180° whole-brain SPECT scan was performed on a dual head γ-camera (Toshiba 7200GCA), with fiducial markers containing 370 kBq (10 μCi) $^{131}$I-TM-601 placed on each zygoma and on the nasion to orient SPECT scans with regard to subsequent MR images. A $^{131}$I-TM-601 standard was also placed ~10 cm above the patient head. Data were acquired at 3° per step at 30 s per step. For these images, a 128 × 128 matrix was used, the high-energy collimator was kept centered at 364 keV with a 15% window, and a ramp filter was applied for 3-dimensional (3D) reconstruction. Data were acquired in a proprietary format and converted to Interfile 3.0 for data analysis. Subsequent SPECT scans were performed with the total-body planar images on days 2, 3, and 4 and on day 6 or day 8 after injection.

### MRI

Postoperative MRI scans were also acquired for each patient before $^{131}$I-TM-601 injections. For each patient, ~20 transverse slices were acquired on a scale of 16 bits per pixel with a matrix size of 256 × 256. Sequences included coronal, axial, and sagittal T1-weighted images (with and without gadolinium contrast), T2 axial, fluid-attenuated inversion recovery (FLAIR), and 3D spoiled gradient echo (3D-SPGR) images. All MRI scans were stored as DICOM (Digital Imaging and Communications in Medicine) files for future image processing and analysis.

### SPECT Image Processing

All image analysis was performed with Analyze 5.0 software (Analyze Direct). For each patient, the SPECT scan, comprised of 128 × 128 × 68 voxels of ~79.5 mm$^3$, for each day (days 1–8) was loaded on Analyze 5.0, with the slices containing the standard excluded. For each SPECT scan, the intensity range on a scale of 32 bits per pixel was calculated and recorded with the expectation that the magnitude (the range of intensity values) of the brightest voxel should correspond roughly to the decay or the dispersion of radioisotope. For the purpose of volumetric analysis, each value was normalized based on the duration of the scans, and the normalized intensities for each patient were then averaged for all patients on each day of scanning. The accuracy of this method was confirmed by comparing the magnitude of the brightest voxel of the standard for 5 patients and the physical decay of $^{131}$I, accomplished by defining a volume of interest (VOI) that included only the standard (the slices removed from the cranial VOI) and measuring the calculated intensities within this VOI. Once normalized and averaged, the intensities were fitted exponentially.

### Formation of MRI Volumes

For each patient, T1-weighted with gadolinium contrast (T1-Wc) and T2 volumes were formed from 2-dimensional images on the Analyze 5.0 platform. Resolution of the coronal and sagittal images was considerably lower than the axial resolution: voxel height was ~7 mm; length and width were ~0.83 mm. Therefore, the volumes were reloaded as linearly interpolated, isotropic voxels of 0.83 × 0.83 × 0.83 mm or around 0.57 mm$^3$. The volumes were primarily analyzed in the axial (transverse) plane.

### Image Analysis: Stereological Estimation of Volume

Tumor volumes for each patient were determined from the T1-Wc, T2, and SPECT scans. Given the arbitrary nature of gray-scale threshold methods and the substantial differences that result in volumes of extracted objects (*19*), stereological Cavalieri sections were used in Analyze 5.0 (*20*). One of every 3 slices was sampled for each scan, and the highlighted or tumor-associated region was demarcated.

A reasonable minimum volume was determined via the exclusion of ambiguous sample points; a reasonable maximum volume was determined via inclusion of those sample points. The mean was then calculated for each volume with the accompanying error equal to half the spread between the recorded minimum and maximum. In addition, for SPECT scans (where limited resolution of $^{131}$I rounds-off tumor extent), a full width at half maximum (FWHM) was intermittently calculated across the cross-sectional diameter (transverse plane) using the Line Profile option, with the assumption that intensity falloff would more-or-less follow a normal (gaussian) curve. The diameter of the stereological volume was then checked by the sampled FWHM for accuracy.

For MR images, 2 volumes were determined for each patient: T1-Wc and T2 estimates of tumor. For SPECT, the tumor volumes for the second day after injection and the final day were catalogued for each patient.

### Coregistration

After separate image processing, the isotropic MR volumes were coregistered to the SPECT scan volumes using Analyze 5.0. Under the 3D Registration program, SPECT scans were matched manually and fused to MR images for each patient, using the alignment of fiducial markers on each SPECT volume to the identifiable anatomic structures of the nasion and zygoma on the MR image. Both the base MR volume and the matched SPECT volume had to be displayed with adjusted scaling: For the MR image, this meant narrowing the intensity window to increase contrast; for the SPECT image, the intensity window was narrowed until highlighted voxels corresponded with measured FWHM measurements and, in addition, gray-scale intensities were converted to a 24-bit red, green, blue (RGB) color-map "hot body" for visual affect.

## RESULTS

### Treatment Response and Toxicity

Therapeutic response and toxicity to $^{131}$I-TM-601 will be presented in detail in a separate publication. To summarize, a total of 18 patients were treated at 3 institutions over a period of 14 mo. There were no $^{131}$I-TM-601–related deaths or grade III–IV toxicities. No patients were withdrawn from the study. The median survival for the cohort was 8.1 mo

**TABLE 1**
Biodistribution Estimates Based on Total-Body Planar Images

| Patient no. | Biologic $t_{1/2}$ (h) | | | | | | | Peak %ID measured ~1 h for brain/cavity and ~24 h for other organs | | | | | |
|---|---|---|---|---|---|---|---|---|---|---|---|---|---|
| | Body | Stm/spln | L kidney | R kidney | Thyroid | Contralateral brain | Tumor cavity | Stm/spln | L kidney | R kidney | Thyroid | Contralateral brain | Tumor cavity |
| 1 | 30.70 | 20.10 | 20.10 | 22.60 | 70.60 | 34.50 | 25.00 | 1.21 | 0.67 | 0.62 | 1.13 | 4.95 | 76.54 |
| 2 | 38.56 | 23.97 | 32.18 | 23.41 | 54.60 | 36.96 | 27.90 | 3.63 | 1.35 | 1.95 | 0.11 | 2.55 | 91.30 |
| 3 | 49.70 | 21.71 | 22.65 | 23.12 | 51.22 | 47.16 | 46.20 | 3.27 | 0.50 | 0.69 | 0.12 | 3.81 | 90.50 |
| 4 | 38.60 | 23.97 | 32.18 | 23.41 | 54.60 | 36.96 | 27.90 | 0.72 | 0.73 | 0.71 | 0.16 | 4.65 | 75.57 |
| 5 | 81.01 | 18.95 | 28.19 | 24.93 | 1,000 | 79.67 | 80.23 | 2.19 | 0.54 | 0.49 | 0.09 | 3.61 | 77.26 |
| 6 | 41.58 | 26.41 | 27.61 | 30.98 | 159.92 | 43.74 | 37.43 | 1.10 | 0.35 | 0.36 | 0.20 | 1.78 | 84.29 |
| 7 | 40.81 | 27.14 | 25.40 | 23.09 | 60.87 | 30.86 | 24.61 | 4.33 | 0.55 | 0.81 | 0.13 | 3.78 | 96.89 |
| 8 | 50.13 | 17.32 | 24.85 | 33.21 | 35.31 | 41.79 | 40.25 | 0.46 | 0.17 | 0.23 | 0.06 | 4.56 | 93.45 |
| 9 | 49.78 | 25.87 | 30.94 | 31.79 | 144.97 | 54.50 | 41.67 | 2.62 | 0.79 | 0.80 | 0.17 | 4.74 | 74.99 |

Stm/spln = stomach/spleen.

compared with 4 mo for historical controls. There were 3 complete responses to treatment, and all 3 patients remain disease free at 17–21 mo after treatment. A phase II trial of $^{131}$I-TM-601 is currently underway.

### Biodistribution

Total-body planar scans were used to estimate effective half-lives in organs visible above the background body tissue. In these scans, the amount of radioactivity present in any given organ was determined by converting counts in the region of the interest to radioactivity using the calibrated standard at the feet of each patient. Using geometric mean quantification and the $^{57}$Co transmission scan for attenuation correction, the percentage of injected dose (%ID) and biologic half-life ($t_{1/2}$) were calculated. Using these methods, in the present subset of 9 patients, these $t_{1/2}$ values were calculated as 47 ± 5 h for bodily elimination, 45 ± 5 h for elimination from the brain, and 39 ± 6 h for elimination from the cavity (Table 1).

For all 9 patients, retention of radiolabeled peptide was observed in the tumor cavity region for the duration of scans. This was illustrated in the total-body planar scans on day 2 and days 6–8 (Fig. 1).

All SPECT scans also showed clear evidence of $^{131}$I-TM-601 remaining at the tumor site on days 6–8 at an activity comparable to that of the 37-MBq (1 mCi) standard. For the standard, the decay rate of the value of the brightest voxel roughly followed the rate of physical decay (Fig. 2). The calculated exponential of the standard yielded a $t_{1/2}$ of ~6.3 ± 1 d, slightly shorter than the known $t_{1/2}$ for $^{131}$I of 8.04 d.

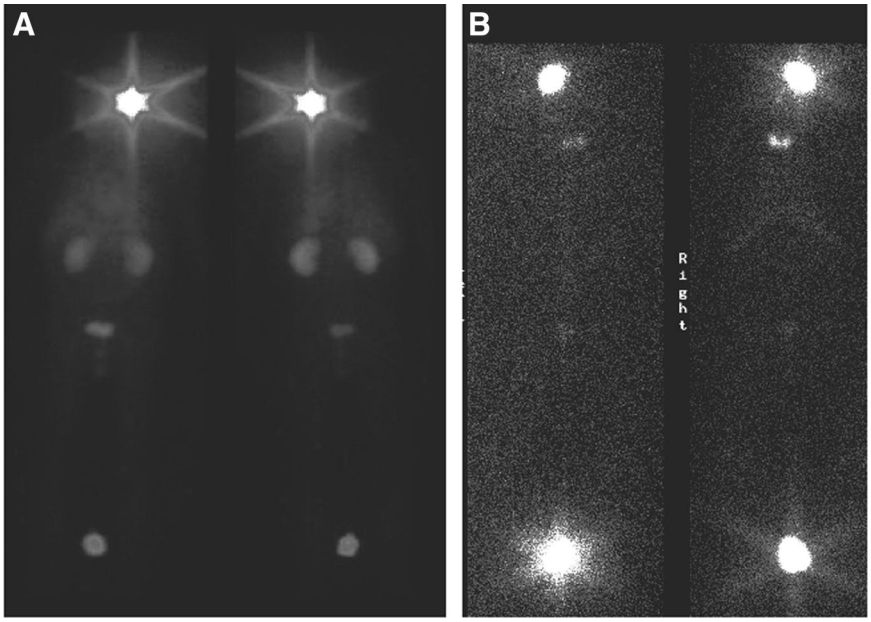


**FIGURE 1.** Total-body planar images show distribution of $^{131}$I-TM-601 immediately after injection (A) and 8 d later (B). Long-term retention of radioactivity at tumor site, with nearly complete elimination elsewhere, was observed in all patient scans. The 7.4-MBq (200 μCi) standard is at bottom.

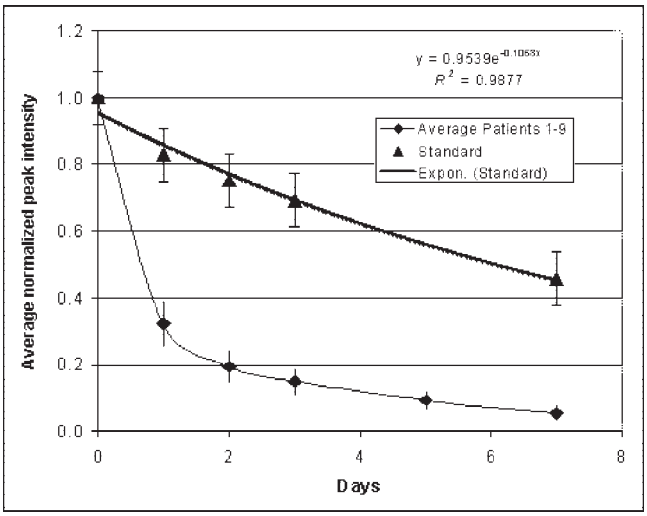


**FIGURE 2.** Graph of average SPECT decay shows that normalized intensity of brightest voxel averaged over all patients drops significantly in 2 d. Expon. = exponential physical decay of 7.4-MBq (200 μCi) sample of $^{131}$I-Tm-601 standard over data collection period.

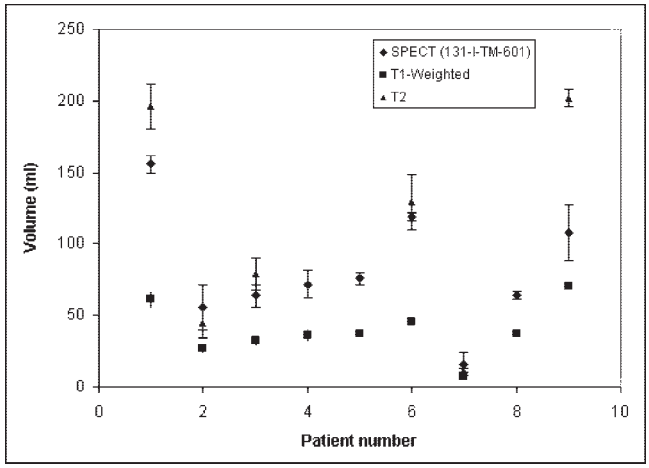


**FIGURE 4.** Comparison of T1-weighted MRI-, T2-weighted MRI-, and SPECT-determined tumor volume estimates on day 8. SPECT day 2 estimates exhibit more uncertainty and generally larger volumes than those on day 8. SPECT day 8 estimates are more centered (but still closer to T2 estimate) and more reliable.

### Tumor Volume

Stereological estimation of tumor volumes in the 9 patients showed that $^{131}$I-TM-601–estimated volumes were intermediate, between the T1-Wc–estimated volumes on the low end and the T2-determined volumes on the high end. Over the course of scanning, the estimated volume 24 h after injection was significantly larger and above or equal to T2 estimates for most patients; by 6–8 d after injection, most peptide-determined volumes were smaller, better centered between T1-Wc and T2 volumes, and considerably less uncertain (Figs. 3 and 4).

SPECT-determined volumes on day 2 and days 6–8 were always larger than the T1-Wc–determined volumes, and most were smaller than the T2-determined volumes by day 8. Moreover, FWHM measures across the span of the SPECT volume corresponded with the smaller volumes of day stereological estimates on day 8.

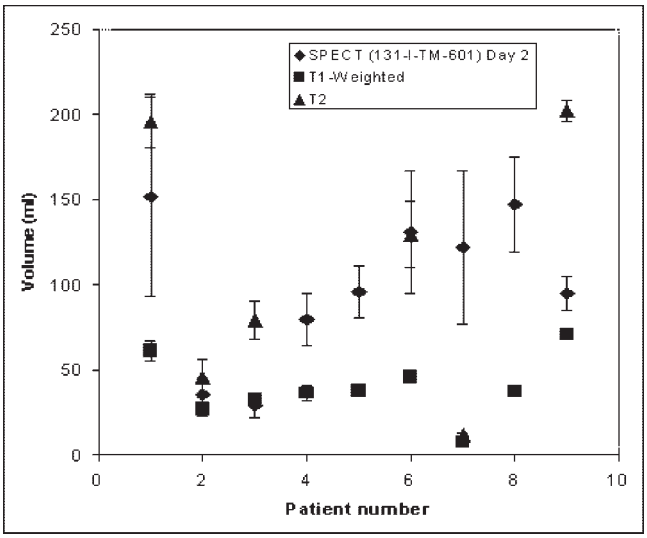


**FIGURE 3.** Comparison of T1-Wc MRI-, T2-weighted MRI-, and SPECT-determined tumor volume estimates on day 2.

### Coregistration of Images

The coregistration of SPECT volumes to MR images via the use of fiducial markers yielded high-overlap and well-centered regions of tumor extent 168 h after injection (Fig. 5).

As the SPECT-estimated volumes were rounded, they tended to approximate the area around the edema (contrast enhancing on T1-Wc) and necrotic region (dark center on T1-Wc) and resection area (also dark) and extend to regions in the T2-determined volume. Generally, the SPECT-determined volume was centered in this region and agreed with the highlighted T1-Wc and T2 areas.

SPECT images performed on day 1 exhibited overwhelming scatter and were not useful for image analysis. By day 2, coregistered images showed considerable isolation of the highlighted SPECT region to that of the tumor region on the MR image (Fig. 6). Further differentiation was evident on day 3, with the SPECT-determined volume better centered and shifted from the site of injection and the cavity toward the necrotic core. By day 8, residual scatter from the cavity and injection site had vanished and the remaining radiolabeled isotope had an intensity level comparable to the standard.

## DISCUSSION

### Tumor Volumes

For the present study, $^{131}$I was chosen for its potential therapeutic benefit compared with less energetic but better imaging radioisotopes such as $^{123}$I or $^{124}$I. Because of the

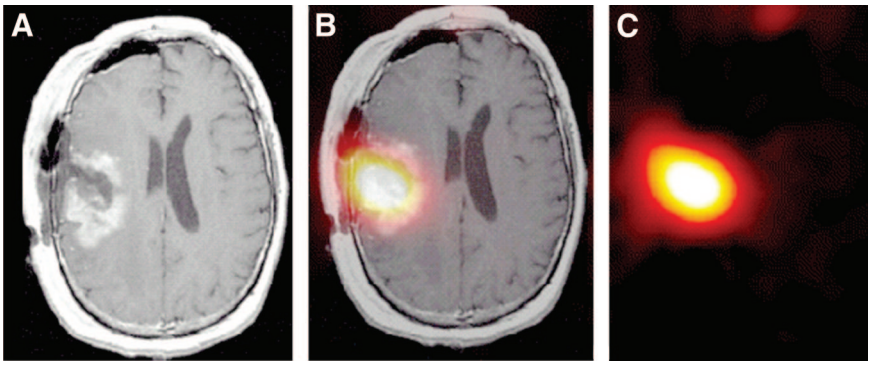


**FIGURE 5.** Axial view of T1-Wc (A), coregistered (B), and SPECT (day 8) images.

substantial Compton scatter partly due to collimator septal penetration from high-energy photons (637 and 722 keV) from $^{131}$I, difficulty arises in defining the exact tumor extent. Stereological methods offer better statistical estimates and more reproducible results than traditional threshold methods when the exact extent of the region of interest is unknown (*19–21*). As a practical measure, stereology also allows the sampling of a smaller number of slices with the same or better accuracy than region-of-interest drawing. Therefore, as far as $^{131}$I is concerned, the volume of distribution of TM-601 is best estimated from stereology. Of course, other radioisotopes that have better imaging characteristics may allow more precise methods to be used in the foreseeable future.

The SPECT-estimated volumes of distribution must be approached with several factors in mind. SPECT-estimated volumes appear rounded-off due to the limited spatial resolution of the γ-camera. The pixel size of our SPECT was 4.3 mm. In addition, detailed structural features are further smeared due to the scatter. Consequently, the cavity shape appeared to be spheric or ellipsoid, despite the more irregular appearance in T1-Wc or T2 MRI, and the uncertainty of the estimate is generally large.

Similar qualifications exist for MRI-determined volumes, where the tumor per se is estimated by regions of enhancement caused by increased capillary permeability. These areas may consist of tumor but may also demonstrate postoperative or radiation-induced effects or inflammatory changes. Generally, for T1-Wc, the glioma tumor volume is underestimated as the invasive fringe tumor cells lack the increased angiogenesis necessary to register in this modality. In contrast, T2 signal hyperintensity may represent tumor or radiation-induced vasogenic edema, infiltrating tumor, or cytotoxic effects and, as such, T2 estimates tend to exaggerate the true extent of tumor.

In the present study, SPECT-determined volumes using $^{131}$I-TM-601 appear to provide better estimates than T1-Wc– or T2-determined estimates. The larger volume and uncertainties in day 2 stereological estimates corresponded with the presence of more diffusely highlighted voxels than in day 8, where the steep falloff allowed the highlighted SPECT volume to be readily discernible. Substantial septal penetration diminished resolution beyond practicality for the initial day, and no distinguishable trends could be registered within the interval of a day—that is, the volumes on consecutive days were effectively the same. By day 8, this uncertainty had diminished substantially and the volumes were more easily estimated, since a sample marker could be readily identified as belonging to the set of volume points. Therefore, lower energy imaging isotopes of higher spatial resolution may provide substantially better tumor definition.

On the whole, SPECT-estimated volumes were smaller on day 8, suggesting that the nonbound radiolabeled peptide is rapidly eliminated from the brain, whereas bound peptide persists for at least several days. The volumes are hedged between the stereologically estimated T1-Wc and T2 volumes. Most SPECT volumes were in fact closer to the T2 estimate than the T1-Wc estimate by day 8, suggesting that $^{131}$I-TM-601 diffuses and binds to at least a portion of the invasive tumor cells in the surrounding parenchyma. The

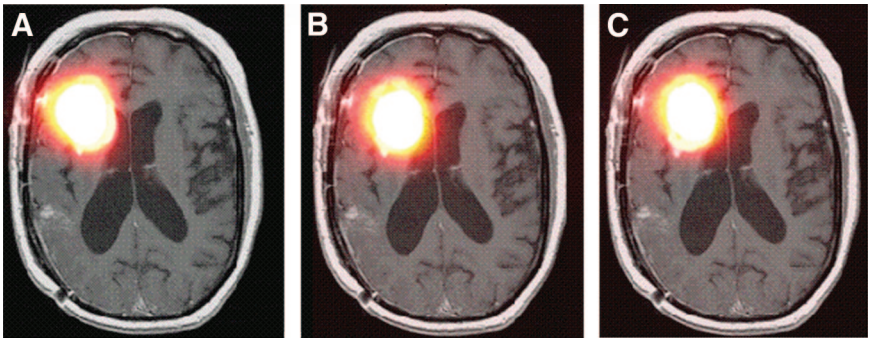


**FIGURE 6.** Coregistered MR/SPECT images for patient 5 on day 2 (A), day 3 (B), and day 8 (C) after injection.

biologic decay rate indicates ongoing biologic elimination via either enzymatic cleavage of iodine, release of peptide from the tumor site, or peptide degradation. Nonetheless, the amount of biologic elimination is relatively small, suggesting long-term retention of intact radiolabeled peptide at the tumor. This observation should be tempered by the limited resolution and high-energy scatter caused by $^{131}$I, which prevents a spatially accurate assessment of the true extent of distribution of the peptide.

### Overlap of Coregistered Volumes

The detailed anatomic clarity of MRI coregistered to SPECT scans allows more accurate differentiation of actual tumor and imaging artifacts than seen in the SPECT scans alone. The increased utility of image coregistration is well documented and likely to be important in determining the utility of this peptide for long-term use. Other imaging technologies such as "digital subtraction" (*22*) may also prove useful in increasing the imaging sensitivity with TM-601.

Biometric analysis of planar images, overlap of SPECT- and MRI-determined volumes in coregistration, and peak intensity decay indications together corroborate evidence of the robust binding of TM-601 to glioma cells in parenchyma proximate to the surgically created resection cavity. Moreover, the sum of present data suggests the stability of the radioligand up to 168 h after injection and the decay of the bound radioisotope through primarily physical processes rather than biologic elimination.

## CONCLUSION

The specificity and stability of $^{131}$I-TM-601 allowed adequate imaging of high-grade gliomas with superb localization but limited resolution in the clinical setting. These findings are promising and encourage the development of higher resolution radioligands of TM-601 such as $^{124}$I or $^{64}$Cu for PET. SPECT-determined volumes using $^{131}$I-TM-601 appear to provide better estimates than T1-Wc– or T2-determined estimates, and the coregistration of MRI and SPECT images suggests that $^{131}$I-TM-601 reliably estimates the extent of primary brain tumor. Due to the impracticality of administering an imaging agent via intracranial injection, the imaging capabilities of this compound after intravenous injection will be important to assess.

## ACKNOWLEDGMENTS

We thank Tisha Cruz for manuscript preparation, Mireya Sanchez and Tammy Klothymonsup for assistance with patient care–related issues, and Rachelle Padilla for expertise in image processing. We also thank the City of Hope General Clinical Research Center for nursing support. Financial support was provided by the Sol Smith and Ruth Cagan Foundations, the City of Hope Cancer Center, and Transmolecular, Inc.

## REFERENCES

1. Central Brain Tumor Registry of the United States (CBTRUS). *Statistical Report: Primary Brain Tumors in the United States, 1992–1997.* Hinsdale, IL: CBTRUS; 2000.
2. American Brain Tumor Association. Facts & statistics. In: *Primer on Brain Tumors.* Des Plaines, IL: American Brain Tumor Association; 2001.
3. Brady L, Miyamoto C, Woo DV, et al. Malignant astrocytomas treated with iodine-125 labeled monoclonal antibody 425 against epidermal growth factor receptor: a phase II trial. *Int J Radiat Oncol Biol Phys*. 1992;22:225–230.
4. Natali PG, Nicotra M, Bigotti R, et al. Comparative analysis of the expression of the extracellular matrix protein tenascin in normal human fetal, adult and tumor tissues. *Int J Cancer*. 1991;47:811–816.
5. Debinski W, Obiri NI, Powers SK, Pastan I, Puri RK. Human glioma cells overexpress receptors for interleukin 13 and are extremely sensitive to a novel chimeric protein composed of interleukin 13 and pseudomonas exotoxin. *Clin Cancer Res.* 1995;1:1253–1258.
6. Ricci PE, Karis JP, Heiserman JE, Fram EK, Bice AN, Drayer BP. Differentiating recurrent tumor from radiation necrosis: time for re-evaluation of positron emission tomography? *AJNR*. 1998;19:407–413.
7. Kahn D, Follett KA, Bushnell DL, et al. Diagnosis of recurrent brain tumor: value of $^{201}$Tl SPECT vs $^{18}$F-fluorodeoxyglucose PET. *AJR*. 1994;163:1459–1465.
8. Lin A, Bluml S, Mamelak AN. Efficacy of proton magnetic resonance spectroscopy in clinical decision making for patients with suspected malignant brain tumors. *J Neurooncol*. 1999;45:69–81.
9. Butzen J, Prost R, Chetty V, et al. Discrimination between neoplastic and nonneoplastic brain lesions by use of proton MR spectroscopy: the limits of accuracy with a logistic regression model. *AJNR*. 2000;21:1213–1219.
10. Adamson AJ, Rand SD, Prost RW, Kim TA, Schultz C, Haughton VM. Focal brain lesions: effect of single-voxel proton MR spectroscopic findings on treatment decisions. *Radiology*. 1998;209:73–78.
11. Soroceanu L, Gillespie Y, Khazaeli MB, Sontheimer H. Use of chlorotoxin for targeting of primary brain tumors. *Cancer Res*. 1998;58:4871–4879.
12. Dittrich K, Power AP, Smith NA. Scorpion sting syndrome: a ten year experience. *Ann Saudi Med*. 1995;15:148–155.
13. Piantadosi S. Clinical trials as experimental designs. In: *Clinical Trials: Methodology Perspectives.* New York, NY: Wiley; 1997.
14. Bigner DD, Brown MT, Friedman AH, et al. Iodine-131-labeled antitenascin monoclonal antibody 81C6 treatment of patients with recurrent malignant gliomas: phase I trial results. *J Clin Oncol*. 1998;16:2202–2212.
15. Soroceanu L, Manning TJ Jr, Sontheimer H. Modulation of glioma cell migration and invasion using $Cl^-$ and $K^+$ ion channel blockers. *J Neurosci*. 1999;19:5942–5954.
16. Ullrich N, Bordey A, Gillespie GY, Sontheimer H. Expression of voltage-activated chloride currents in acute slices of human gliomas. *Neuroscience*. 1998;83:1161–1173.
17. Ullrich N, Gillespie GY, Sontheimer H. Human astrocytoma cells express a unique chloride current. *Neuroreport*. 1996;7:1020–1024.
18. Woltanski KP, Besch W, Keilacker H, Ziegler M, Kohnert KD. Radioiodination of peptide hormones and immunoglobulin preparations: comparison of the chloramine T and Iodogen method. *Exp Clin Endocrinol*. 1990;95:39–46.
19. Rajapakse JC. Random-grid stereologic volumetry of MR head scans. *J Magn Reson Imaging*. 2000;12:833–841.
20. Roberts N, Puddephat MJ, McNulty V. The benefit of stereology for quantitative radiology. *Br J Radiol.* 2000;73:679–697.
21. Gadeberg P, Gundersen HJ, Tagehoj F. How accurate are measurements on MRI? A study on multiple sclerosis using reliable 3D stereological methods. *J Magn Reson Imaging*. 1999;10:72–79.
22. O'Brien, TJ, So EL, Mullan BP, et al. Subtraction ictal SPECT co-registered to MRI improves clinical usefulness of SPECT in localizing the surgical seizure focus. *Neurology*. 1998;50:445–454.